Optimised photometric stereo via non-convex variational minimisation

Laurent Hoeltgen, Yvain Quéau, Michael Breuss, Georg Radow

Optimised photometric stereo via non-convex variational minimisation

Laurent Hoeltgen[1]
hoeltgen@b-tu.de
Yvain Quéau[2]
yvain.queau@enseeiht.fr
Michael Breuß[1]
breuss@b-tu.de
Georg Radow[1]
radow@b-tu.de

[1] Chair for Applied Mathematics
BTU Cottbus-Senftenberg,
Cottbus, Germany

[2] IRIT, UMR CNRS 5505
Université de Toulouse
Toulouse, France

Abstract

Estimating the shape and appearance of a three dimensional object from flat images is a challenging research topic that is still actively pursued. Among the various techniques available, Photometric Stereo (PS) is known to provide very accurate local shape recovery, in terms of surface normals. In this work, we propose to minimise non-convex variational models for PS that recover the depth information directly. We suggest an approach based on a novel optimisation scheme for non-convex cost functions. Experiments show that our strategy achieves more accurate results than competing approaches.

1 Introduction

Photometric 3D-reconstruction techniques are often formulated as inverse problems: given an image I, one seeks a depth map z that best explains the observed grey levels of the data. To this end we use the image irradiance equation (IIE) $I(u,v) = \mathcal{R}(z(u,v);s,\rho)$ where $(u,v) \in \Omega$ represents pixel coordinates over the reconstruction domain $\Omega \subseteq \mathbb{R}^2$. This model describes the interactions between the surface z and the lighting s; ρ representing the reflectance parameters (*e.g.* the albedo), which can be either known or considered as hidden unknown parameters. For the sake of simplicity, we will consider only Lambertian reflectance without shadows, and we assume that the lighting of a photographed scene is directional and known.

The Shape-from-Shading (SfS) problem consists in solving the IIE over Ω. Unfortunately, this is an ill-posed problem, even with simple reflectance models such as Lambertian reflectance with known albedo. To eliminate the inherent ambiguities of classic SfS, several images I^i, $i \in \{1,\dots,m\}$, can be considered under different lightings s^i, $i \in \{1,\dots,m\}$. PS consists in finding a depth map z that best explains all IIEs:

$$I^i(u,v) = \mathcal{R}(z(u,v);s^i,\rho), \qquad i \in \{1,\dots,m\} \tag{1}$$

In this work, we aim at obtaining the solution z of the PS problem, see Figure 1 for an account. We will show that estimating the optimal solution necessarily involves non-trivial optimisation

Example input image for PS

$\mathcal{E}_{\mathcal{R}} = 13.78$
Classic PS with integration

$\mathcal{E}_{\mathcal{R}} = 3.50$
Our method

Figure 1: From a set of $m \geq 3$ images (cf. left), classic PS provides an albedo and a normal map which best explain the input images in the sense of a local, pointwise estimation. In a second step, the smooth depth map is estimated by integration. Yet, the final surface is not the best explanation of the images, as indicated by the reprojection error $\mathcal{E}_{\mathcal{R}}$ (c.f. energy in (5)) (middle). We display this using white for $2.5 \cdot 10^{-3}$ and black for zero. Instead of this local procedure, we propose to minimise the reprojection criterion in terms of the depth and the albedo, through global non-convex optimisation. Not only the images are better explained (right), but we also demonstrate that the 3D-reconstruction results are improved (cf. Section 4).

methods, even with the simplest models for the reflectance function $\mathcal{R}$ (Lambertian, without shadows) and the deviations from this model (additive, zero-mean, Gaussian noise). We propose a numerical framework to approximate an optimal solution, which can be used to refine classic PS results. Our approach relies on matrix differential theory for analytic derivations and on recent developments in non-convex optimisation.

2 Construction of our method and related work

Following Woodham [27] it is known that, provided $m \geq 3$ input images and non-coplanar calibrated lightings are given, all surface normals can be estimated without ambiguity. In addition, the reflectance parameters (*e.g.* the albedo) can also be estimated. This is usually achieved by minimising the difference between the given data (the input images) and the reprojection according to the estimated normal and albedo:

$$\min_{n,\rho} \left\{ \mathcal{E}_{\mathcal{R}}^{\text{local}}(n,\rho;I) := \frac{1}{m} \sum_{(u,v)\in\Omega} \sum_{i=1}^{m} \Phi\left(I^i(u,v) - \mathcal{R}\left(n(u,v); s^i, \rho(u,v)\right)\right) \right\} \tag{2}$$

with an estimator Φ. As a result, one obtains an approximation of the normal $n(u,v)$ and the albedo $\rho(u,v)$ at each position (u,v). These estimates are the optimal local explanations of the image, in the sense of the estimator Φ. Yet, the estimated normal field is in general not integrable. Thus, the depth map that can be obtained by integration is not an optimal image explanation, but only a smooth explanation of the noisy normal field, cf. Figure 1.

Instead of this pointwise joint estimation of the normal and the albedo, it is possible to employ photometric ratios: dividing the i-th by the j-th IIE in (1), one obtains a homogeneous linear system in each normal vector that does not depend on the albedo. The least squares estimate of Wu *et al.* [29] yields the Maximum Likelihood (ML) estimate if the ratios are corrupted by additive, zero-mean, Gaussian noise. However, any noise hypothesis should be made on the images, and not on their ratios. Since the ratio of two Gaussian random variables

follows a Cauchy distribution [7], approaches based on ratios only provide the best linear unbiased estimate (BLUE), which is not the optimal (efficient) estimator. Besides, there is no reason why the estimated normal field should be integrable.

As indicated, the normal field computed by this type of local PS approaches does not need to be integrable. Hence, the integration task is usually formulated as another optimisation problem, aiming at minimising the discrepancy between the estimated normal field and that of the recovered surface. Assuming orthographic projection, the relation between the normal $n(u,v)$ and the depth $z(u,v)$ is given by:

$$n(u,v) := \frac{1}{\sqrt{\|\nabla z(u,v)\|^2+1}}\left[-\nabla z(u,v),\,1\right]^\top \quad \text{where} \quad \nabla z = (z_u, z_v)^\top \tag{3}$$

Then the best smooth surface explaining the computed normals can be estimated either by solving (3) by means of an eikonal-type equation [1], or by solving the variational problem:

$$\min_z \left\{ \mathcal{E}_{\text{integ}}(z;n) := \sum_{(u,v)\in\Omega}\sum \Psi\left(\left\| \nabla z(u,v) - \begin{bmatrix} -n_1(u,v)/n_3(u,v) \\ -n_2(u,v)/n_3(u,v) \end{bmatrix} \right\|^2 \right) \right\} \tag{4}$$

where Ψ is again some estimator function (see [4, 6] for some discussion).

One may realise that, at this stage of the process chain of PS with integration, the images are not considered anymore. Thus, the final surface is in general not optimal in the sense of the reprojection criterion. Regularising the normal field before integration [23, 30] may also ensure integrability, but since such methods only use the normal field, and not the images, they can obviously not guarantee optimality with respect to the reprojection either.

Global PS approaches solve the latter problem as they represent a way to ensure that the recovered surface is optimal with respect to the reprojection criterion. Moreover, it is possible to solve the system (1) directly in terms of the depth [3]: this ensures both that the recovered surface is regular, and that it is optimal with respect to the reprojection criterion, calculated from the depth map z and not from a non-integrable estimate of its gradient. Some PDE-based PS approaches have been recently proposed, and were shown to ease the resolution in particularly difficult situations such as pointwise lightings, specular reflectance [26] and multi-view PS [5]. To ensure robustness, such methods can be coupled with variational methods [13, 22, 25]. In other words, the criterion which should be considered for ensuring optimality of a surface reconstruction by PS is not the local criterion (2), but rather:

$$\min_{z,\rho} \left\{ \mathcal{E}_{\mathcal{R}}(z,\rho;I) := \frac{1}{m}\sum_{(u,v)\in\Omega}\sum\sum_{i=1}^{m} \Phi\left(I^i(u,v) - \mathcal{R}\left(z(u,v); s^i, \rho(u,v)\right)\right) \right\} \tag{5}$$

A theoretical analysis of the choice $\Phi(x) = |x|$, in the continuous setting, can be found in [2]. Numerical resolution methods based on proximal splittings were more recently introduced in [21]. Yet, this last work relies on an "optimise then discretise" approach which would involve non-trivial oblique boundary conditions (BC), replaced there for simplicity reasons by Dirichlet BC. Obviously, this represents a strong limitation which prevents working with many real-world data where this BC is rarely available.

The normal vectors n^i defined as in (3) and involved in the reflectance function $\mathcal{R}$ have unit length. As a consequence, the optimisation problem (5) is non-linear and non-convex. The ratio procedure described earlier can be used: it simultaneously eliminates the albedo and the non-linear terms, cf. [5, 22, 25, 26] and obviously removes the bias due to non-integrability. But let us recall that it is only the BLUE estimate, and also not the optimal one.

To guarantee optimality, it is necessary to minimise the non-linear, non-convex energy, *i.e.* without employing ratios.

Solving (5) is a challenging problem. Efficient strategies to find the sought minimum are scarce. Recently Ochs *et al.* [17] proposed a novel method to handle such non-convex optimisation problems, called *iPiano*. A major asset of the approach is the extensive convergence theory provided in [16, 17]. Because of this solid mathematical foundation we explore the iPiano approach in this work. The scheme makes explicit use of the derivative of the cost function, which in our case involves derivatives of matrix-valued functions, and we will employ as a technical novelty, matrix differential theory [11, 12] to derive the resulting scheme.

3 Non-convex discrete variational model for PS

In this section we describe details of our discrete framework for estimating both the depth and the (Lambertian) reflectance parameters over the domain Ω.

3.1 Assumptions on the PS model

We assume $m \geq 3$ grey level images I^i, $i \in \{1,\dots,m\}$, are available, along with the m lighting vectors $s^i \in \mathbb{R}^3$, assumed to be known and non-coplanar. We also assume Lambertian reflectance and neglect shadows, which leads to the following well-known model:

$$\mathcal{R}\left(n(u,v);s^i,\rho\right) := \rho\left(u,v\right)\left\langle s^i, n\left(u,v\right)\right\rangle, \quad (u,v)\in\Omega, \quad i=1,\dots,m \tag{6}$$

where $\rho(u,v)$ is the albedo at the surface point conjugated to pixel (u,v), considered as a hidden unknown parameter. Let us note that real-world PS images can be processed by low-rank factorisation techniques in order to match the linear reflectance model (6), cf. [28].

We further assume orthographic projection, hence the normal $n(u,v)$ is given by (3). Then the reflectance model becomes a function of the depth map z:

$$\mathcal{R}\left(z(u,v);s^i,\rho\right) := \frac{\rho\left(u,v\right)}{\sqrt{\|\nabla z(u,v)\|^2+1}}\left\langle s^i, [-\nabla z(u,v),1]^\top\right\rangle, \quad (u,v)\in\Omega, \quad \forall i \tag{7}$$

Eventually, we assume that the images I^i differ from this reflectance model only up to an additive, zero-mean, Gaussian noise. The ML estimator is thus the least-squares estimator $\Phi(x)=\frac{1}{2}x^2$, and the cost function in the reprojection criterion (5) becomes:

$$\mathcal{E}_{\mathcal{R}}\left(z,\rho;I\right) := \frac{1}{2m}\sum_{(u,v)\in\Omega}\sum_{i=1}^{m}\left(I^i(u,v)-\frac{\rho(u,v)}{\sqrt{\|\nabla z(u,v)\|^2+1}}\left\langle s^i,[-\nabla z(u,v),1]^\top\right\rangle\right)^2 \tag{8}$$

3.2 Tikhonov regularisation of the model

Our energy in (8) only depends on the gradient ∇z and not on the depth z itself. As a consequence, solutions can only be determined up to an arbitrary constant. As a remedy we follow [22] and introduce a reference depth z_0, thus regularising our initial model with a zero-th order Tikhonov regulariser controlled by a parameter $\lambda > 0$:

$$\min_{z,\rho}\left\{\mathcal{E}_{\mathcal{R}}\left(z,\rho;I\right)+\frac{\lambda}{2}\sum_{(u,v)\in\Omega}\left(z(u,v)-z_0(u,v)\right)^2\right\} \tag{9}$$

In practice, λ can be set to any small value, so that the minimiser of (9) lies as close as possible to a minimiser of (8). In all our experiments we set $\lambda := 10^{-6}$ and z_0 as the classic PS solution followed by least-squares integration.

3.3 Discretisation

As already mentioned, "optimise then discretise" approaches such as [21] for solving (9) involve non-trivial BC. Hence, we prefer a "discretise then optimise", finite dimensional formulation of the variational PS problem (9). In our discrete setting we are given m images I^i, $i \in \{1,\dots,m\}$, with n pixels labelled with a single index j running from 1 to n. We rewrite (9) in the following way:

$$\underset{z,\rho\in\mathbb{R}^n}{\arg\min}\left\{\frac{1}{2m}\sum_j \left\| I_j - \frac{\rho_j}{\sqrt{\|\nabla z_j\|^2+1}} S \begin{bmatrix} -\nabla z_j \\ 1 \end{bmatrix} \right\|^2 + \frac{\lambda}{2}\|z_j - z_{0\,j}\|^2 \right\} \tag{10}$$

where $I_j := [I_j^1,\dots,I_j^m]^\top \in \mathbb{R}^m$ is the vector of intensities at pixel j, ∇z_j represents again a finite difference approximation of the gradient of z at pixel j, and $S = [s^1,\dots,s^m]^\top \in \mathbb{R}^{m,3}$ is a matrix containing the stacked m lighting vectors s^i.

We remark that the matrix S can be decomposed into two sub-matrices S_ℓ and S_r of dimensions $m\times 2$ and $m\times 1$ such that $S := \begin{bmatrix} S_\ell & S_r \end{bmatrix}$, and so that

$$S \begin{bmatrix} -\nabla z_j \\ 1 \end{bmatrix} = -S_\ell \nabla z_j + S_r \tag{11}$$

Let us also introduce a $2n\times n$ block matrix M, such that each block M_j is a $2\times n$ matrix containing the finite difference coefficients used for approximating the gradient:

$$M := \begin{bmatrix} M_1 & \dots & M_n \end{bmatrix}^\top \in \mathbb{R}^{2n,n}, \qquad M_j z \approx \nabla z_j \in \mathbb{R}^2 \tag{12}$$

We further introduce the following aliases:

$$A_j(z,\rho) := -\frac{\rho_j}{\sqrt{1+\|M_j z\|^2}} S_\ell \in \mathbb{R}^{m,2}, \qquad b_j(z,\rho) := I_j - \frac{\rho_j}{\sqrt{1+\|M_j z\|^2}} S_r \in \mathbb{R}^m \tag{13}$$

and stack them, respectively, in a block-diagonal matrix and a vector:

$$A(z,\rho) := \begin{bmatrix} A_1(z,\rho) & & \\ & \ddots & \\ & & A_n(z,\rho) \end{bmatrix} \in \mathbb{R}^{mn,2n}, \qquad b(z,\rho) := \begin{bmatrix} b_1(z,\rho) \\ \vdots \\ b_n(z,\rho) \end{bmatrix} \in \mathbb{R}^{mn} \tag{14}$$

Using these notational conventions the task in (10) can be rewritten compactly as

$$\underset{z,\rho\in\mathbb{R}^n}{\arg\min}\left\{ \underbrace{\frac{1}{2m}\|A(z,\rho)Mz - b(z,\rho)\|_2^2}_{:=f(z,\rho)} + \underbrace{\frac{\lambda}{2}\|z - z_0\|_2^2}_{:=g(z)} \right\} \tag{15}$$

which is the discrete PS model we propose to tackle in this paper. Let us remark that this model can be easily extended to include more realistic reflectance [10] and lighting [18] models, as well as more robust estimators [9]: this only requires to change the definition of f, which stands for the global reprojection error $\mathcal{E}_\mathcal{R}$.

3.4 Alternating optimization strategy

In order to ensure applicability of our method to real-world data, the albedo ρ cannot be assumed to be known. Inspired by the well-known Expectation-Maximisation algorithm, we treat ρ as a hidden parameter, and opt for an alternating strategy which iteratively refines the depth with fixed albedo, and the hidden parameter with fixed depth:

$$z^{(k+1)} = \arg\min_z \left\{ f\left(z, \rho^{(k)}\right) + g(z) \right\}, \rho^{(k+1)} = \arg\min_\rho \left\{ f\left(z^{(k+1)}, \rho\right) + g\left(z^{(k+1)}\right) \right\} \quad (16)$$

starting from $z^{(0)} = z_0$ and taking as $\rho^{(0)}$ the albedo obtained by the classic PS approach [27]. Of course, the choice of a particular prior z_0 has a direct influence on the convergence rate of the algorithm. The proposed scheme globally converges towards the solution even with a trivial prior $z_0 \equiv$ constant, but convergence is very slow in this case. Thus the proposed method should be considered as a post-processing technique to refine classic PS approaches, rather than as a standalone PS method.

Now, let us comment on the two optimisation problems in (16). Updating ρ amounts to a linear least-squares problem which admits the following closed-form solution at each pixel:

$$\rho_j^{(k+1)} = \sqrt{1 + \|M_j z^{(k+1)}\|^2} \sum_{i=1}^m I_j^i s^{i\top} \begin{bmatrix} -M_j z^{(k+1)} \\ 1 \end{bmatrix} \Bigg/ \sum_{i=1}^m \left(s^{i\top} \begin{bmatrix} -M_j z^{(k+1)} \\ 1 \end{bmatrix} \right)^2 \quad (17)$$

The computation of $z^{(k+1)}$ is considerably harder, and it is dealt with below.

3.5 The iPiano algorithm

We will now formulate the iPiano algorithm for our problem. Since the albedo is fixed for the purpose of the corresponding optimisation stage, we denote $f(z) = f(z, \rho^{(k)})$. The iPiano algorithm seeks a minimiser of

$$\min_{x \in \mathbb{R}^n} \{ f(x) + g(x) \} \quad (18)$$

where $g\colon \mathbb{R}^n \to \mathbb{R}$ is convex and $f\colon \mathbb{R}^n \to \mathbb{R}$ is smooth. What makes iPiano appealing is the fact that g must not necessarily be smooth and f is not required to be convex. This allows manifold designs of novel fixed-point schemes. In its general form it evaluates

$$\mathrm{prox}_{\alpha g} \left(z^{(k)} - \alpha \nabla f(z^{(k)}) + \beta (z^{(k)} - z^{(k-1)}) \right) \quad (19)$$

where the proximal operator is given by

$$\mathrm{prox}_{\alpha g}(z) := \arg\min_x \left\{ \frac{1}{2} \|x - z\|^2 + \alpha g(x) \right\} \quad (20)$$

and which goes back to Moreau [15]. Before we can define the final algorithm we also need to approximate the gradient of f.

3.6 Gradient of f

In our setting the main difficulty is that the matrix A depends on our sought unknown z. In order to state a useful representation of this gradient we have to resort to matrix differential calculus. We refer to [11, 12, 19, 20] for a more in-depth representation. A key notion is the definition of the Jacobian of a matrix, which can be obtained in several ways. We follow [11].

Definition 1 (Jacobian of a Matrix Valued Function)**.** *Let A be a differentiable $m \times p$ real matrix function of an $n \times q$ matrix X of real variables,* i.e. $A = A(X)$. *The* Jacobian matrix *of A at X is the $mp \times nq$ matrix*

$$D[A](X) := \frac{\mathrm{d}\,\mathrm{vec}\,(A(X))}{\mathrm{d}(\mathrm{vec}\,X)^\top} \tag{21}$$

where $\mathrm{vec}\,(\cdot)$ *corresponds to the vectorisation operator described in [8] (Definition 4.29). This operator stacks column-wise all the entries from its matrix argument to form a large vector.*

Here, differentiability of a matrix valued function means that the corresponding vectorised function is differentiable in the usual sense. By this definition the computation of a matrix Jacobian can be reduced to computing a Jacobian for a vector valued function. In extension of this definition one can easily derive matrix-valued versions of the standard product- and chain-rule from calculus (cf. Theorem 7 and 9 in [11]). Let us state directly our main result, details on its proof can be found in the supplementary material.

Theorem 1. *Using matrix differential theory we obtain for the gradient of f:*

$$\nabla f(z) = \frac{1}{m}\left(A(z)M + \left((Mz)^\top \otimes I_{nm}\right) D[A](z) - D[b](z)\right)^\top (A(z)Mz - b(z)) \tag{22}$$

Here, I_{nm} represents the identity matrix in $\mathbb{R}^{nm,nm}$ and the symbol $\otimes$ stands for the Kronecker matrix product [8] (Definition 4.2.1).

Equation (22) is computationally expensive to evaluate. If run times are an important criterion, then one may use the following approximation, motivated by (22):

$$\nabla f(z) \approx \frac{1}{m}(A(z)M)^\top (A(z)Mz - b(z)) \tag{23}$$

We conjecture that this is an efficient way to approximate $\nabla f(z)$ for computations. In our numerical experiments, we used (23) and could not observe any deficiencies.

Our final algorithm for the computation of the depth and the albedo is given in Algorithm 1. For our experiments, the iPiano stopping criterion was set to a test on the relative change in the objective function ($< 10^{-8}$), and the global stopping criterion to a maximum number of iterations. For the step sizes we employed the "lazy backtracking" algorithm as in [17].

4 Numerical Evaluation

Figure 2 presents the test data that we use in this paper. It consists of five real-world scenes captured under 20 different known illuminants s^i, $(i = 1, \ldots, 20)$, provided in [24]. In our experiments, we used $m = 20$ out of the original 96 RGB images, which we converted to grey levels. Two of the sets present diffuse reflectance (*Cat* and *Pot*), while two other exhibit broad specularities (*Bear* and *Buddha*) and one presents sparse specular spikes (*Ball*). Since the ground truth normals are also provided in [24], the estimated normals can be computed from the final depth map according to (3), and compared to the exact ground truth. For evaluation, we indicate the Mean Angular Error (MAE) (in degrees) over the reconstruction domain Ω. Let us consider the *Cat* data set in some detail, as it consists in a diffuse scene that fits

Algorithm 1: Inertial Proximal Point Algorithm for Photometric Stereo

Choose prior z_0 (classic PS), prior weight λ (10^{-6}), $\beta \in [0,1[$ (0.5) and $c > 0$ (0.01)
Initialise $z^{(0)}$ (z_0) and $\rho^{(0)}$ (classic PS), and set $k = 0$
repeat
  Set $\tilde{z}^{(0)} = \tilde{z}^{(-1)} = z^{(k)}$ and $l = 0$
  repeat
    Lipschitz constant L estimation by lazy backtracking
    Step size update: $\alpha^{(l)} = 2\frac{1-\beta}{c+L}$
    Depth update: $\tilde{z}^{(l+1)} = \text{prox}_{\alpha^{(l)} g}\left(\tilde{z}^{(l)} - \alpha^{(l)} \nabla f\left(\tilde{z}^{(l)}\right) + \beta\left(\tilde{z}^{(l)} - \tilde{z}^{(l-1)}\right)\right)$
    $l = l + 1$
  until *iPiano convergence*
  $z^{(k+1)} = \tilde{z}^{(l+1)}$
  Albedo update using Eq. (17)
  $k = k + 1$
until *global convergence*

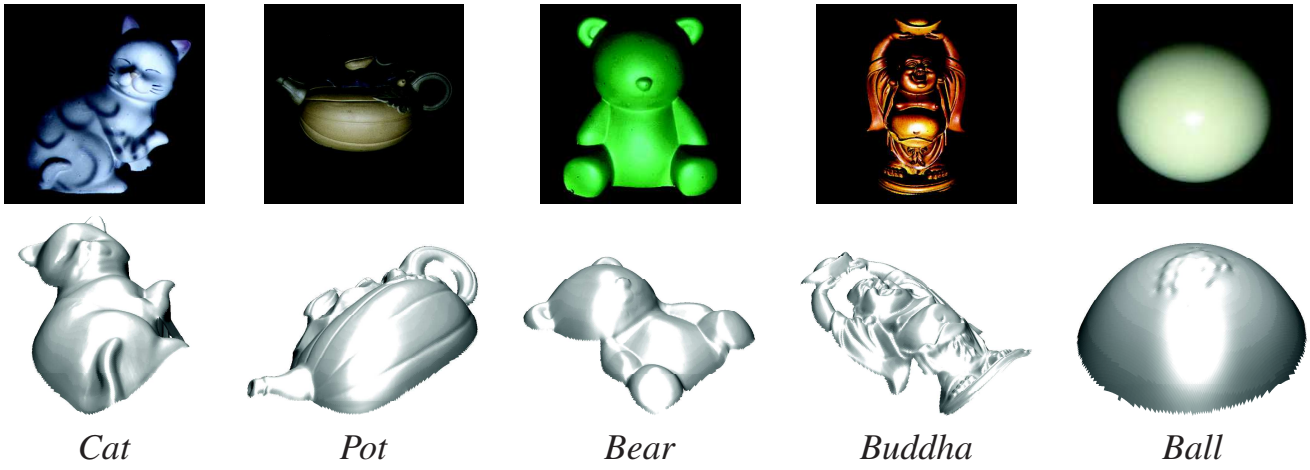

Figure 2: Test data (brightened and cropped to enhance visualisation) and 3D-reconstructions obtained after 500 iterations k of Algorithm 1.

rather well our assumptions. We let our algorithm run for 1000 iterations k (approx. 1 hour on a recent i7 processor, using non-optimised Matlab code), and study the evolution of two criteria: the reprojection error, whose minimum is sought by our algorithm; and the MAE, which indicates the overall accuracy of the 3D-reconstruction, cf. the two left images within Figure 3. The displayed convergence graphs indicate that each iteration from Algorithm 1 not only decreases the value of the objective function $f + g$ (which is approximately equal to the reprojection error $\mathcal{E}_\mathcal{R} = f$), but also the MAE. This confirms our conjecture that finding the best possible explanation of the images yields more accurate 3D-reconstructions. In the other two graphs in Figure 3 we study the results of our method compared to other PS strategies based on least-squares: the classical PS framework [27] consisting in estimating in a least squares sense the normals and the albedo, and integrating them afterwards, and the recent differential ratios procedure from [22, 25]. The latter allows direct recovery of the depth, but on the other hand it changes the objective function. Both other approaches rely on linear least squares: they are thus by far faster than the proposed approach (here, a few seconds, versus a few minutes with ours). Yet, in terms of accuracy, these methods are outperformed by our

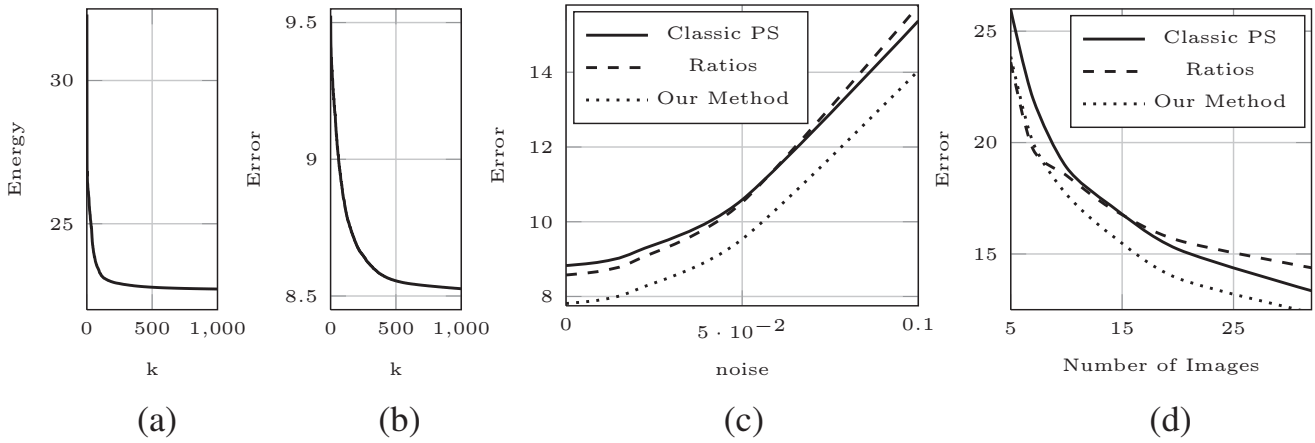

Figure 3: The *Cat* experiment (from left to right): (a) objective function $f + g$ as a function of the iterations count k; (b) MAE between the reconstructed surface and the ground truth; (c) reprojection error for competing methods for increasing noise levels (we indicate the standard deviation of the additive, zero-mean Gaussian noise, as a percentage of the maximum intensity); (d) ditto for increasing numbers of input images, with 0.1 noise level.

Table 1: Reconstruction errors (MAE, in degrees) obtained for preprocessed input images using the approach from [28]. For fair comparison, the MAE for classic PS is calculated on the final surface, *i.e.* using the normals calculated by finite differences from the final depth map, rather than the (non-integrable) normals estimated in the first step. Regarding the ratio procedure, we applied the code from [22] directly on the grey level data.

	Cat	Pot	Bear	Buddha	Ball
Classic PS [27]	8.83	8.91	7.01	14.34	3.05
Differential ratios [22]	8.57	9.00	7.01	14.31	3.13
Our method (500 iterations)	**7.81**	**8.57**	**6.90**	**13.90**	**2.97**

approach, no matter the noise level or the number of images (which were preprocessed via low-rank factorization [28] in these two experiments).

By making the input images Lambertian via low-rank preprocessing [28], we can make a reasonable comparison for the whole test dataset. Table 1 shows that our postprocessing method can still improve the accuracy. The 3D-reconstruction results obtained with the full pipeline are shown in Figure 4. In comparison with Figure 2, artefacts due to specularities are clearly reduced.

5 Conclusions

We have shown the benefits of high performing numerical methods in the context of photometric stereo. Let us emphasise that only by such novel numerical methods complex models as arising in PS can be handled with success. Our results show that a significant quality gain can be achieved in this way. A more detailed view on the computational results reveals that remaining inaccuracies seem to be mostly due to shadows and highlights, edges and depth discontinuities. Thus, an interesting perspective of our work would be to use more robust estimators, which would ensure both robustness to outliers [9] and edges preservation [4].

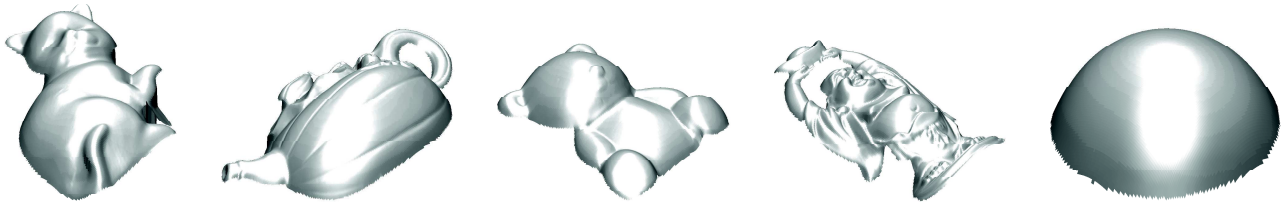

Figure 4: 3D-reconstruction results using the *full pipeline*, consisting of a preprocessing [28], followed by classic PS [27], and finally the proposed method.

References

[1] M. Bähr and M. Breuß. An improved eikonal method for surface normal integration. In *German Conference on Pattern Recognition (GCPR)*, volume 9358 of *Lecture Notes in Computer Science*, pages 274–284. Springer International Publishing, 2015.

[2] J. Chabrowski and Z. Kewei. On variational approach to photometric stereo. *Annales de l'Institut Henri Poincaré (C) Analyse non linéaire*, 10(4):363–375, 1993.

[3] J. J. Clark. Active photometric stereo. In *IEEE Conference on Computer Vision and Pattern Recognition (CVPR)*, pages 29–34, 1992.

[4] J.-D. Durou, J.-F. Aujol, and F. Courteille. Integrating the normal field of a surface in the presence of discontinuities. In *Energy Minimization Methods in Computer Vision and Pattern Recognition (EMMCVPR)*, volume 5681 of *Lecture Notes in Computer Science*, pages 261–273. Springer, 2009.

[5] P. F. U. Gotardo, T. Simon, Y. Sheikh, and I. Matthews. Photogeometric scene flow for high-detail dynamic 3D reconstruction. In *Proc. IEEE Int. Conf. Computer Vision (ICCV)*, pages 846–854, 2015.

[6] M. Harker and P. O'Leary. Regularized reconstruction of a surface from its measured gradient field. *Journal of Mathematical Imaging and Vision*, 51(1):46–70, 2015.

[7] D. V. Hinkley. On the ratio of two correlated normal random variables. *Biometrika*, 56 (3):635–639, 1969.

[8] R. A. Horn and C. R. Johnson. *Topics in Matrix Analysis*. Cambridge University Press, 1994.

[9] S. Ikehata, D. Wipf, Y. Matsushita, and K. Aizawa. Photometric stereo using sparse Bayesian regression for general diffuse surfaces. *IEEE Transactions on Pattern Analysis and Machine Intelligence*, 36(9):1816–1831, 2014.

[10] Y.-C. Ju, S. Tozza, M. Breuß, A. Bruhn, and A. Kleefeld. Generalised Perspective Shape from Shading with Oren-Nayar Reflectance. In *Proceedings of the British Machine Vision Conference*, 2013.

[11] J. R. Magnus and H. Neudecker. Matrix differential calculus with applications to simple, Hadamard, and Kronecker products. *Journal of Mathematical Psychology*, 29:474–492, 1985.

[12] J. R. Magnus and H. Neudecker. *Matrix Differential Calculus with Applications in Statistics and Econometrics*. John Wiley & Sons, 3rd edition, 2007.

[13] R. Mecca and Y. Quéau. Unifying diffuse and specular reflections for the photometric stereo problem. In *Proc. IEEE Winter Conf. Applications of Computer Vision (WACV)*, pages 1–9, 2016.

[14] R. Mecca, A. Wetzler, A. M. Bruckstein, and R. Kimmel. Near field photometric stereo with point light sources. *SIAM Journal on Imaging Sciences*, 7(4):2732–2770, 2014.

[15] J. J. Moreau. Proximité et dualité dans un espace Hilbertien. *Bulletin de la Société Mathématique de France*, 93:273–299, 1965.

[16] P. Ochs. Unifying abstract inexact convergence theorems for descent methods and block coordinate variable metric ipiano. Technical report, Saarland University, 2016.

[17] P. Ochs, Y. Chen, T. Brox, and T. Pock. iPiano: Inertial proximal algorithm for non-convex optimization. *SIAM Journal on Imaging Sciences*, 7(2):1388–1419, 2014.

[18] Thoma Papadhimitri and Paolo Favaro. Uncalibrated near-light photometric stereo. In *Proceedings of the British Machine Vision Conference*, 2014.

[19] K. B. Petersen and M. S. Pedersen. The matrix cookbook, 2012. Available from https://www.math.uwaterloo.ca/~hwolkowi/matrixcookbook.pdf.

[20] D. S. G. Pollock. Tensor products and matrix differential calculus. *Linear Algebra and Its Applications*, 67:169–193, 1985.

[21] Y. Quéau, F. Lauze, and J.-D. Durou. A l1-tv algorithm for robust perspective photometric stereo with spatially-varying lightings. In *Scale Space and Variational Methods in Computer Vision (SSVM)*, volume 9087 of *Lecture Notes in Computer Science*, pages 498–510, 2015.

[22] Y. Quéau, R. Mecca, and J.-D. Durou. Unbiased photometric stereo for colored surfaces: a variational approach. In *IEEE Conference on Computer Vision and Pattern Recognition (CVPR)*, 2016.

[23] D. Reddy, A. Agrawal, and R. Chellappa. Enforcing integrability by error correction using l^1-minimization. In *IEEE Conference on Computer Vision and Pattern Recognition (CVPR)*, 2009.

[24] B. Shi, Z. Wu, Z. Mo, D. Duan, S.-K. Yeung, and P. Tan. A benchmark dataset and evaluation for non-Lambertian and uncalibrated photometric stereo. In *IEEE Conference on Computer Vision and Pattern Recognition (CVPR)*, 2016.

[25] W. Smith and F. Fang. Height from Photometric Ratio with Model-based Light Source Selection. *Computer Vision and Image Understanding*, 145:128–138, 2016.

[26] S. Tozza, R. Mecca, M. Duocastella, and A. Del Bue. Direct differential photometric stereo shape recovery of diffuse and specular surfaces. *Journal of Mathematical Imaging and Vision*, 56(1):57, September 2016. ISSN 1573-7683.

[27] R. J. Woodham. Photometric method for determining surface orientation from multiple images. *Optical Engineering*, 19(1):134–144, 1980.

[28] L. Wu, A. Ganesh, B. Shi, Y. Matsushita, Y. Wang, and Y. Ma. Robust photometric stereo via low-rank matrix completion and recovery. In *Asian Conference on Computer Vision (ACCV)*, volume 6494 of *Lecture Notes in Computer Science*, pages 703–717. Springer Berlin Heidelberg, 2010.

[29] T.-P. Wu, K. L. Tang, C.-K. Tang, and T. T. Wong. Dense Photometric Stereo: A Markov Random Field Approach. *IEEE Transactions on Pattern Analysis and Machine Intelligence*, 28(11):1830–1846, 2006.

[30] B. Zeisl, C. Zach, and M. Pollefeys. Variational regularization and fusion of surface normal maps. In *International Conference on 3D Vision (3DV)*, 2014.